Relation between time reversal focusing and coherent backscattering in multiple scattering media: A diagrammatic approach

Julien de Rosny,* Arnaud Tourin, and Arnaud Derode
Laboratoire Ondes et Acoustique, CNRS/ESPCI/Université Paris VII, UMR 7587, 10 rue Vauquelin, 75005 Paris, France

Bart van Tiggelen
Laboratoire de Physique et Modélisation des Milieux Condensés, CNRS/Maison de Magistères, Université Joseph Fourier Boîte Postale 166, 38042 Grenoble Cedex 9, France

Mathias Fink
Laboratoire Ondes et Acoustique, UMR 7587, CNRS/ESPCI/Université Paris VII, 10 rue Vauquelin, 75005 Paris, France
(Received 1 March 2004; published 5 October 2004)

In this paper, we revisit one-channel time reversal (TR) experiments through multiple scattering media in the framework of the multiple scattering theory. The hyperresolution and the self-averaging property are retrieved. The developed formalism leads to a deeper understanding of the role of the ladder and most-crossed diagrams in a TR experiment and also establishes the link between TR and coherent backscattering (CBS). Especially, we show that when the initial source and the time reversal point are at the same location, the time-reversed amplitude is twice higher. Surprisingly, this enhancement is due to the ladder diagrams and not to the most-crossed ones, contrary to CBS. These theoretical predictions are confirmed by experimental results. The experiments are performed with ultrasonic waves propagating through a random collection of parallel steel rods.

DOI: 10.1103/PhysRevE.70.046601 PACS number(s): 43.20.+g, 43.35.+d, 73.20.Fz, 42.25.Dd

I. INTRODUCTION

A few years ago, we carried out the first experimental demonstration of the reversibility of acoustic waves propagating through a two-dimensional (2D) random collection of scatterers, the ultrasonic equivalent of a Lorentz gas for particles [1]. Typically, an ultrasonic source sends a broadband pulse into a medium consisting of thousands of parallel steel rods randomly distributed and immersed in water. Since the mean free path is much less than the sample thickness, strong multiple scattering occurs. The multiply scattered signals transmitted through the medium are recorded on a 128-transducer array, digitized and time reversed. A part of the signal, the so-called "time reversal window," is transmitted back into the medium. The time-reversed wave is found to converge back to its source. Two aspects of this problem have been studied: the signal recreated at the source location (time compression) and the spatial focusing of the time-reversed wave around the source location which was found to show a finer spatial resolution than in a homogeneous medium (hyperfocusing). Dowling and Jackson [2] have been pioneers in this field: three years before the first experimental observation, they predicted the peculiar property of hyperfocusing of time reversal in random media. But their approach was restricted to narrow-band signals and time compression was thus not expected. Later we developed a phenomenological statistical model to describe both spatial and temporal focusing of a broadband pulse [3–5]. As to Blomgren and Papanicolaou [6], they applied the Green's function formalism to analyze the spatiotemporal focusing obtained by time reversal in a random medium with weak celerity fluctuations. However, their model was based on the parabolic (or paraxial) approximation [7] which assumes only small scattering angles and thus ignores backscattering. In this latter paper, the reason why the focusing is observed for one realization of disorder is referred to as "pulse stabilization." It comes from the "self-averaging" behavior of the time reversal due to the broadband character of the initial pulse.

In the present paper we revisit time reversal (TR) experiments in the framework of the multiple scattering theory. This theory describes statistical moments of the scattered field in transmission as well as in backscattering. It has been extensively applied in several fields of physics (optics, electronics, acoustics, etc.). It is a general theoretical framework that successfully describes various multiple scattering phenomena: diffusive field fluctuations and their application to diffusive-wave spectroscopy (DWS) [8,9], weak and strong localization [10,11], short- and long-range intensity correlations (C_1, C_2, C_3) [12], etc. It was only very recently that arguments based on multiple scattering theory have been proposed in order to explain some results of TR in random media [13]. For simplicity, we focus in this paper on time reversal performed with one transducer. We first present experimental results obtained in backscattering configuration. Hyperresolution and self-averaging are clearly observed in such a configuration. In addition one of the most striking results of this paper is shown: the time reversal amplitude is twice larger when the time reversal element and the initial source positions are the same. Measurements of the mean and the variance of the TR field clearly indicate that this

*Electronic address: julien.derosny@espci.fr

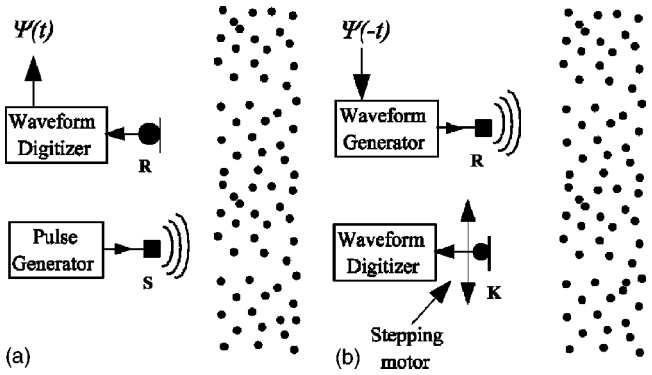

FIG. 1. The two steps of a one-channel TR experiment through a multiple scattering medium in a backscattering configuration. (a) Forward propagation step. (b) Backward propagation step.

effect is closely related to the well-known coherent backscattering (CBS) effect [14,15]. To explain all these experimental results, we have developed a theory whose main steps are the following.

(i) The TR field and its square are deduced from the Green's function formalism on a *single realization* of disorder.

(ii) *Averaging* over realizations: the general expression for the average and the variance of the TR amplitude is expressed in terms of the vertex function.

(iii) Approximation of the vertex: introduction of the ladder and crossed diagrams contributions.

(iv) Analysis of TR in the transmission and backscattering configurations.

(v) Discussion about the self-averaging and hyperresolution properties of TR in a multiple scattering medium.

(vi) The link with the well-known coherent backscattering effect is formally established. In peculiar we show that the enhancement in TR focusing is due to the ladder diagrams and not to the most-crossed ones, contrary to CBS.

II. EXPERIMENTAL RESULTS

An acoustic wave field can be time reversed using a time reversal mirror (TRM). A TRM is usually made of 128 independent time reversal channels. Each channel consists of a piezoelectric transducer plugged to a digital emitting and recording electronics. In this article, we only deal with one-channel TR experiments performed through multiple scattering media. Indeed, the physics in such a configuration is already sufficiently new, rich, and complex to devote the complete study to this topic. The schematic view of the one-channel TR setup is presented in Fig. 1 The experiments have been carried out in a 2D-like multiple scattering medium made of thousands of steel rods. The sample is 35 mm thick and 300 mm large. There are 18.75 rods per square centimeter and the diameter of each rod is 0.8 mm. The elastic mean free path is about 4 mm [16]. The time reversal experiment is divided in two steps. First, a small emitter (here a piezoelectric transducer) located at point **S** generates a short ultrasonic pulse at a central frequency of 3.5 MHz (0.43 mm wavelength) with a 100% bandwidth toward the

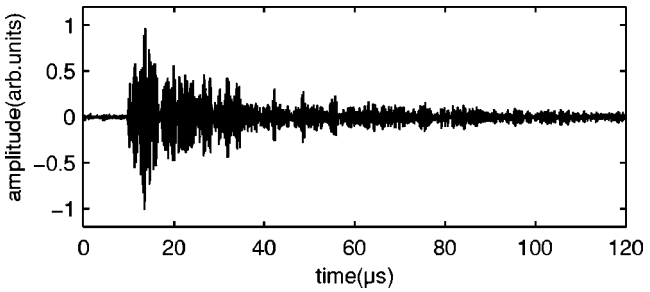

FIG. 2. A typical time evolution for the pressure field recorded at point **R** after the emission of a short 1-μs pulse (at a central frequency of 3.5 MHz) at point **S**.

multiple scattering medium. Another piezoelectric transducer acting as a small microphone records the time dependence of the backscattered wave field, $\Psi(t)$, at point **R**. A typical backscattered signal is plotted in Fig. 2. Since the sample thickness is much larger than the mean free path, the huge time spreading (more than 100 μs) of the initial pulse is due to multiple scattering. Second, the recorded signal is time reversed and sent back into the medium by the transducer at point **R** now acting as a small loudspeaker. Finally a small transducer plugged to a wave form digitizer records the time dependence of the back-propagated pressure field at point **K**. This transducer is fixed on a stepping motor in order to build the spatial map of the TR field around the initial source location. As expected, when **K**=**S**, a short pulse emerges that corresponds to the time-reversed initial pulse (cf. Figs. 3 and 4). This result is obtained for a single realization of disorder. In order to get an estimator for the average TR field, the experiment can be repeated for many other configurations of the scatterer positions. From a practical point of view, averaging is achieved by translating the disordered medium. After averaging, the sidelobe level is decreased but the shape of the compressed pulse seems unchanged (see Fig. 3). This result illustrates the self-averaging property of broadband time reversal in random media. Moreover, we observe in Fig. 4 that the hyper focusing property of TR through complex media is achieved: the focal spot is very thin (2 mm—i.e., 4 wavelengths) whereas no spatial focusing would occur in free space with one single TR channel.

So far the source position and the time reversal channel were assumed to be far away from each other. Do the TR

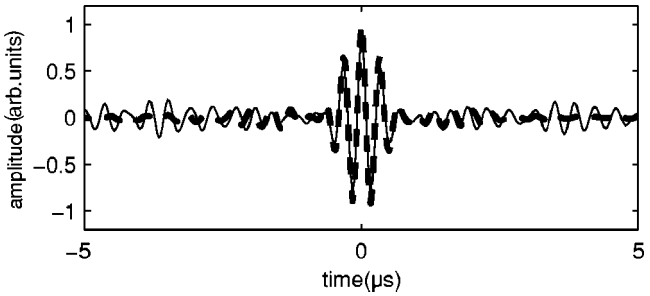

FIG. 3. The continuous line corresponds to the time compression recorded at the initial source position (**K**=**S**) for one realization of disorder. The dotted line is the average value over 100 realizations of disorder. The signals are normalized by the maximum of the average signal which occurs at $t=0$.

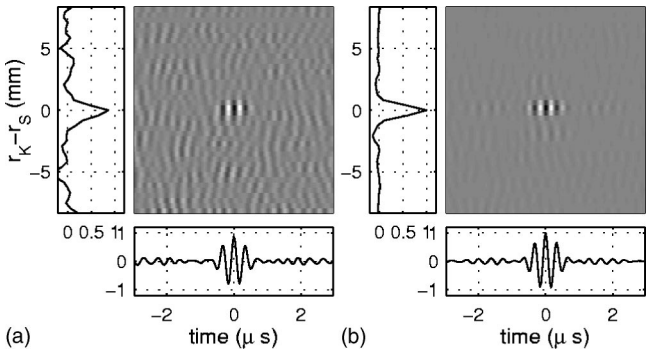

FIG. 4. Spatiotemporal focusing on a single realization of disorder (a) and averaged over 100 realizations (b). The vertical axis corresponds to the distance between the recording point (**K**) and the initial source position (**S**). The signals are normalized by the value of the averaged signal at $t=0$ and $\mathbf{K}=\mathbf{S}$.

focusing characteristics change when points **S** and **R** coincide? An experimental answer comes from Fig. 5. When $\mathbf{S}=\mathbf{K}=\mathbf{R}$, the average TR field is almost twice as large compared to the setup in which **R** and $\mathbf{K}=\mathbf{S}$ are far away from each other. Moreover, if the average TR focusing amplitude is measured as a function of distance between points $\mathbf{S}=\mathbf{K}$ and **R**, the resulting plot looks like the well-known CBS peak (see Fig. 6).

The CBS is a well-known effect occurring in multiple scattering media; it is intimately related to the reciprocity property. When a source located at point **S** emits a short pulse towards a multiple scattering medium, the average backscattered intensity [i.e., $\int\langle\Psi(t)^2\rangle dt$ where $\langle\bullet\rangle$ represents the average over realizations of disorder] received at the source is twice higher than the one received far away. This is due to the constructive interference between each path and its reciprocal counterpart, which can only occur at the source. This phenomenon has been observed in many different areas: in optics, for microwaves, in acoustics, etc. It was first predicted by Watson [17], de Wolf [18], and Barabanenkov [19]. Ten years later, the first experimental evidence of this phenomenon was reported [14,15].

Our preliminary results on time reversal focusing (Figs. 5 and 6) indicate that there is a strong link between TR and CBS. We will later develop a full theoretical analysis to support this statement. Nevertheless, from now on, we propose an intuitive way to explain the link between CBS and TR based on simple physical arguments. Basically, when the source at **S** transmits a Dirac pulse, **R** records the Green's function of the medium between point **S** and **R**, $G(\mathbf{S}\rightarrow\mathbf{R};t)$. This field is time reversed and $G(\mathbf{S}\rightarrow\mathbf{R},-t)$ is sent back into the medium from point **R** to the initial source point, **S**. The back-propagated field on **S** is $G(\mathbf{S}\rightarrow\mathbf{R};-t)\otimes G(\mathbf{R}\rightarrow\mathbf{S};t)$. The reciprocity symmetry of the propagation medium implies that the emission and receiving points can be exchanged in the Green's function—i.e., $G(\mathbf{S}\rightarrow\mathbf{R};t)=G(\mathbf{R}\rightarrow\mathbf{S};t)$. Therefore the TR field is expressed as $\int G^2(\mathbf{S}\rightarrow\mathbf{R},\tau)d\tau$ at the focusing time ($t=0$). This term is just the integrated intensity of the scattered field received at **R** for a source at **S**. Hence, on average, the dependence of the TR amplitude as a function of the TR device position is nothing else than the backscattered intensity pattern—i.e., the coherent backscattering enhancement.

We now perform "dynamic time reversal" experiments; i.e., we do not time reverse the whole signal but only a part of it, the so-called time reversal window. A time reversal window is defined by its length ΔT and its center t_0. First two short time reversal windows ($\Delta T=4$ μs) centered at $t_0=20$ μs and $t_0=40$ μs are selected, time reversed, and successively transmitted back towards the medium. This experiment is repeated for one hundred realizations of disorder and the results are plotted in Fig. 7. Two remarkable properties are observed when $\mathbf{S}=\mathbf{K}$. First, the peak amplitude ($\mathbf{S}=\mathbf{R}$) is twice larger than the background for the two time reversal windows. Second, the width of the peak versus the distance between **S** and **R** seems thinner for the late time reversal window. Systematic measures with respect to t_0 confirm these results. In Fig. 8, we notice that a factor of 2 is measured whatever the time reversal window as soon as there are at least two scattering events. Moreover, the peak width continuously decreases as t_0 increases (see Fig. 9). These two behaviors show the strong link with the dynamic coherent backscattering enhancement [20].

Measuring the variance of the time reversed field is important in order to study the self-averaging property of TR through disordered media. Indeed a process is "self-averaging" if the variance of the field is weak compared to the square of its average value. An experimental map of the variance of the TR field is shown in Fig. 10 when the source point **S** and the single TR channel **R** are far away from each

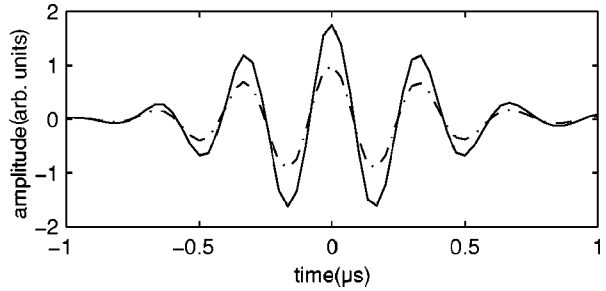

FIG. 5. Average time compression on the initial source ($\mathbf{K}=\mathbf{S}$). Dotted line: the TR device location (**R**) is far from the initial source point(**S**), and its amplitude is normalized to 1. Solid line: they are at the same position ($\mathbf{R}=\mathbf{S}$).

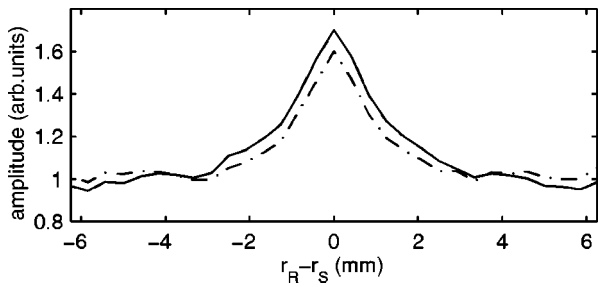

FIG. 6. Solid line: averaged time reversal focusing amplitude (at $t=0$) and $\mathbf{K}=\mathbf{S}$ versus distance between the initial source and the TR device. Dotted line: average backscattered intensity versus distance between the source and the TR device.

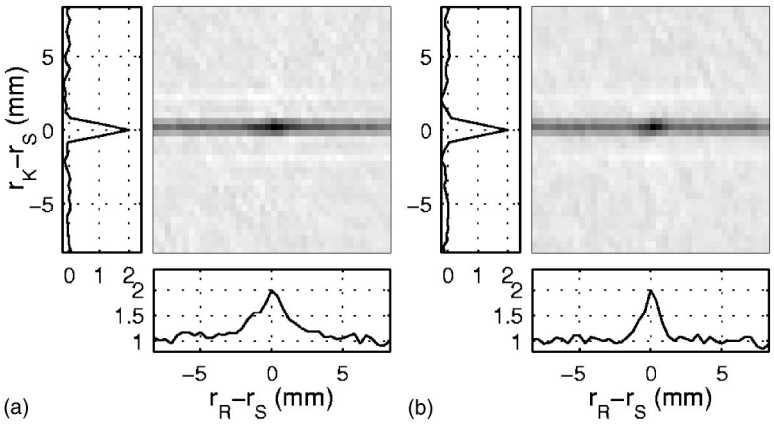

FIG. 7. Gray level representations of the average TR field at time $t=0$ versus the distance between the initial source and the measurement point ($\|\mathbf{S}-\mathbf{K}\|$ on the vertical scale) and the distance between the initial source and the TR channel ($\|\mathbf{S}-\mathbf{R}\|$ on the horizontal scale). (a) and (b) correspond to a 4-μs-long time reversal window centered at time $t_0=20$ μs and $t_0=40$ μs, respectively.

other. Approximately, it seems that two contributions add up to a flat variance that was normalized here to 1. Upon varying the position of the receiver **K**, the first contribution appears around the position of the TR channel **R**. This contribution is seen to be roughly constant in time. The second contribution only occurs at the source position **S** and for times around the focusing time $t=0$. This contribution oscillates twice as fast as the central frequency of the initial pulse. In both cases, the maximum enhancement factor is 2. Figures 11 and 12 confirm these observations.

III. THEORY

A. Time-reversed field

In this part, we formalize the one-channel TR process in terms of the Green's functions. As seen in the preliminary experiment, the first step of a TR experiment begins by the emission of a short pulse $f(t)$ around time $t=0$ by the source located at point **S**. The recorded field Ψ at point **R** is expressed as

$$\Psi(t) = G(\mathbf{S} \to \mathbf{R};t) \otimes f(t), \tag{1}$$

where $\otimes$ is the convolution operator for time variables and $G(\mathbf{S}\to\mathbf{R};t)$ is the Green's function between **S** and **R**.

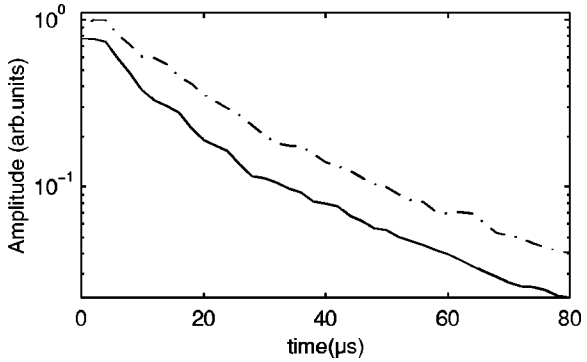

FIG. 8. Amplitude of the average TR field (recorded at time $t=0$ and at the focal position—i.e., $\mathbf{S}=\mathbf{K}$) versus the position of the TR window (t_0). The solid line corresponds to the case where the TR channel is far from the source whereas the dotted line corresponds to the situation where the initial source point and the TR channel are identical.

In order to expand the Green's function, instead of the classical Born expansion in terms of G_0 (Green's function of the unperturbed medium), one can prefer to introduce an operator Θ and the average Green's function G_e—i.e., $\langle G\rangle$. Here G_e is also called the Green's function of the effective medium [21,22]. Then it becomes

$$\Psi(t) = G_e(\mathbf{S} \to \mathbf{R};t) \otimes f(t) + \left[\int G_e(\mathbf{S} \to \mathbf{r}_1;t) \otimes \Theta(\mathbf{r}_1 \to \mathbf{r}_2;t) \otimes G_e(\mathbf{r}_2 \to \mathbf{R};t) d\mathbf{r}_1 d\mathbf{r}_2\right] \otimes f(t). \tag{2}$$

In the following, the first term on the right-hand side of Eq. (2) will be neglected. This is fully justified in a backscattering configuration: the effective Green's function has no specular reflection at the interface because the scatterers den-

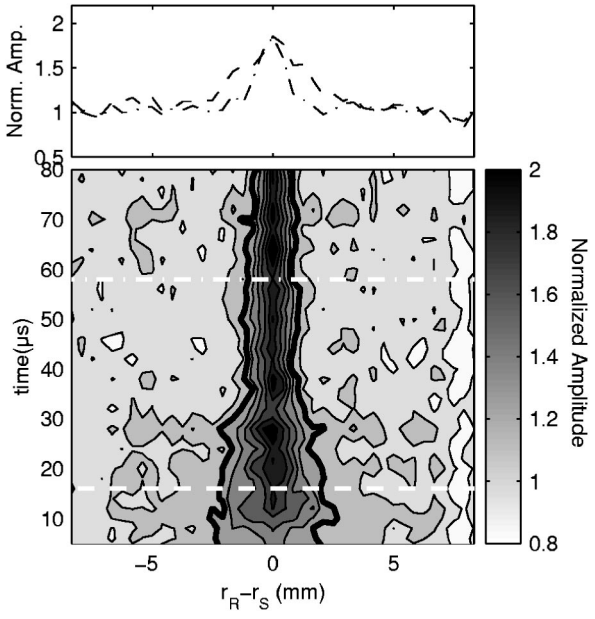

FIG. 9. Average TR focusing peak amplitude at the source ($\mathbf{S}=\mathbf{K}$) versus the distance between the source and the TR channel ($\mathbf{r_R}-\mathbf{r_S}$) and the position t_0 of the TR window. At each time, the field is normalized such that the field equals 1 when **S** and **R** are far apart. The top plot shows two snapshots of the bottom map at times $t_0=17$ μs (dashed line) and $t_0=57$ μs (dash-dotted line).

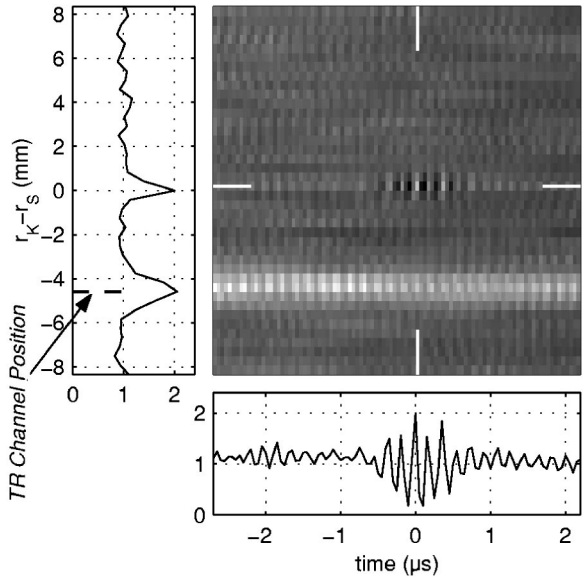

FIG. 10. Gray level representation of the variance of the TR field versus time t (horizontal scale) and versus the distance between the measurement point **K** and the initial source **S** (vertical scale). The TR channel is located at −4.6 mm from the source. The horizontal plot is the time evolution of the variance at the focus (**S**=**K**). The vertical plot is the spatial dependence of the field at $t=0$. The TR window is $\Delta T=2$ μs long and centered at time $t_0=40$ μs.

sity is weak [23] and the ambient fluid is the same in the scattering region and outside. In transmission, this term can also be neglected when the medium is thicker than several elastic mean free paths because the effective Green's function decays exponentially with depth in the multiple scattering medium. In other words, in thick multiple scattering media, almost all the incoming wave is scattered at least once while traveling across the medium. Without the first term on the right-hand side in Eq. (2), the propagation from **S** to **R** can be seen as a three-step process: first, the propagation in the effective homogeneous medium from **S** to $\mathbf{r}_1$; second, the propagation inside the multiple scattering medium between $\mathbf{r}_1$ and $\mathbf{r}_2$; and finally, the propagation from $\mathbf{r}_2$ to **R**, along all possible paths from $\mathbf{r}_1$ to $\mathbf{r}_2$ within the scattering region.

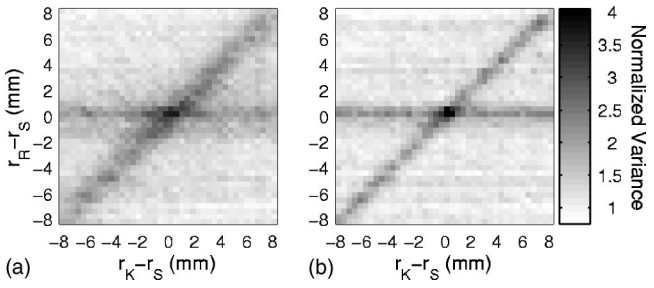

FIG. 11. Variance of the TR field outside the focusing time. The vertical axis corresponds to the distance between the TR channel (**R**) and the source (**S**). The horizontal axis is the distance between the measurement point (**K**) and the source (**S**). The 2-μs-long TR windows are centered around time 20 μs (a) and 40 μs (b), respectively.

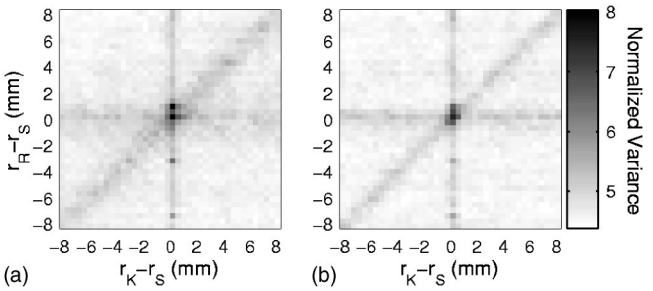

FIG. 12. Variance of the TR field at the focusing time. The vertical axis corresponds to the distance between the TR channel **R** and the source **S**. The horizontal axis is the distance between the measurement point **K** and the source **S**. The TR windows are centered around time 20 μs (a) and 40 μs (b), respectively.

Next, we select a part of the scattered signal, referred to as the time reversal window (TRW):

$$e(t) = A\Psi(t)W\left(\frac{t-t_0}{\Delta t}\right). \tag{3}$$

Here W is the rectangle function.[1] A is an amplitude factor that takes into account a possible amplification, but can be set to unity without loss of generality. The TRW is centered at time t_0 and has a duration ΔT. The selected signal $e(t)$ is time reversed and transmitted back by point **R** through the medium and the field Ψ_{RT} is recorded at point **K** [see Figs. 13(b) and 14(b)]:

$$\Psi_{RT}(t) = e(-t) \otimes G(\mathbf{R} \to \mathbf{K}; t). \tag{4}$$

Combining Eqs. (2)–(4), we obtain

$$\Psi_{RT}(t) = \int \gamma(\mathbf{r}_1,\mathbf{r}_2,\mathbf{r}_3,\mathbf{r}_4;t) \otimes f(-t) \otimes \Theta(\mathbf{r}_3 \to \mathbf{r}_4;t) \otimes \underbrace{\left[W\left(\frac{-t-t_0}{\Delta T}\right)\Theta(\mathbf{r}_1 \to \mathbf{r}_2;-t)\right]}_{\chi_{(t)}} \tag{5}$$

with

$$\gamma(\mathbf{r}_1,\mathbf{r}_2,\mathbf{r}_3,\mathbf{r}_4;t) = G_e(\mathbf{S} \to \mathbf{r}_1;-t) \otimes G_e(\mathbf{R} \to \mathbf{r}_3;t) \otimes G_e(\mathbf{r}_2 \to \mathbf{R};-t) \otimes G_e(\mathbf{r}_4 \to \mathbf{K};t). \tag{6}$$

To obtain Eq. (5) we have assumed that ΔT is larger than the duration of γ, which contains all the effective Green's functions, and χ takes into account propagation inside the disordered medium and the choice of the TRW. Expression (5) for the time-reversed field in terms of G_e and the Θ matrix will serve us as a starting point to work out the average and the variance of the TR field.

[1] $W(x)=1$ if $|x|<1/2$ and $W(x)=0$ if $|x|>1/2$.

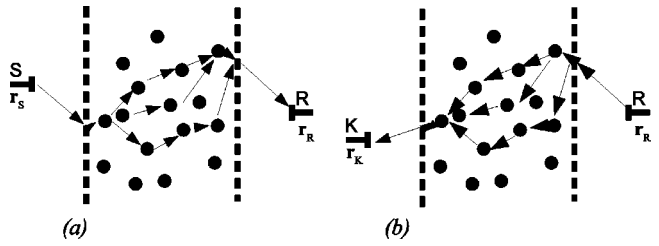

FIG. 13. The two steps of a one-channel TR experiment in transmission through a multiple scattering medium. (a) Forward propagation step. (b) Backward propagation step.

B. Average TR wave field

In Eq. (5), the randomness is contained only in $\chi(t)$. Hence, $\langle\chi(t)\rangle$ is the key to calculate $\langle\Psi_{RT}\rangle$. We have shown that [21]

$$\langle\chi(t)\rangle = \left[\int C_\Theta(\mathbf{r}_1,\mathbf{r}_2;\mathbf{r}_3,\mathbf{r}_4;\tau)W\left(\frac{\tau-t_0}{\Delta T}\right)d\tau\right]\delta(t), \quad (7)$$

where

$$C_\Theta(\mathbf{r}_1,\mathbf{r}_2;\mathbf{r}_3,\mathbf{r}_4;\tau) = \langle\Theta(\mathbf{r}_1\rightarrow\mathbf{r}_2;\tau)\Theta(\mathbf{r}_3\rightarrow\mathbf{r}_4;\tau)\rangle. \quad (8)$$

To obtain Eq. (7) we assumed that in the frequency domain the correlation properties of the Θ operator only depend on the frequency difference. In the multiple scattering theory C_Θ is also referred to as the intensity "vertex" function that links the entry positions $\mathbf{r}_1, \mathbf{r}_3$ to the output ones $\mathbf{r}_2, \mathbf{r}_4$.

We conclude that the average TR field is intimately linked to the intensity vertex according to

$$\begin{aligned}\langle\Psi_{RT}(t)\rangle = \int \gamma(\mathbf{r}_1,\mathbf{r}_2,\mathbf{r}_3,\mathbf{r}_4;t)\otimes f(-t)\\ \times\left[\int C_\Theta(\mathbf{r}_1,\mathbf{r}_2;\mathbf{r}_3,\mathbf{r}_4;\tau)W\left(\frac{\tau-t_0}{\Delta T}\right)d\tau\right]\\ \times d\mathbf{r}_1 d\mathbf{r}_2 d\mathbf{r}_3 d\mathbf{r}_4. \quad (9)\end{aligned}$$

Upon introducing the ξ function,

$$\begin{aligned}\xi_\tau(\mathbf{X}_1,\mathbf{X}_2,\mathbf{X}_3,\mathbf{X}_4;t) = \int G_e(\mathbf{X}_1\rightarrow\mathbf{r}_1;-t)\otimes G_e(\mathbf{r}_2\rightarrow\mathbf{X}_2;-t)\\ \otimes G_e(\mathbf{X}_3\rightarrow r_3;t)\\ \otimes G_e(\mathbf{r}_4\rightarrow\mathbf{X}_4;t)\otimes f(-t)\\ \times C_\Theta(\mathbf{r}_1,\mathbf{r}_2,\mathbf{r}_3,\mathbf{r}_4;\tau)d\mathbf{r}_1 d\mathbf{r}_2 d\mathbf{r}_3 d\mathbf{r}_4, \quad (10)\end{aligned}$$

Eq. (9) reads

$$\langle\Psi_{RT}(t)\rangle = \int \xi_\tau(\mathbf{S},\mathbf{R},\mathbf{R},\mathbf{K};t)W\left(\frac{\tau-t_0}{\Delta T}\right)d\tau. \quad (11)$$

In the following, we will see that the ξ function plays a central role in the multiple scattering theory applied to TR.

From a practical point of view, we often deal with a short time reversal window. When its duration ΔT is sufficiently small so that $C_\Theta(\mathbf{r}_1,\mathbf{r}_2;\mathbf{r}_3,\mathbf{r}_4;\tau)$ is almost constant within this interval, the average TR field can be expressed as

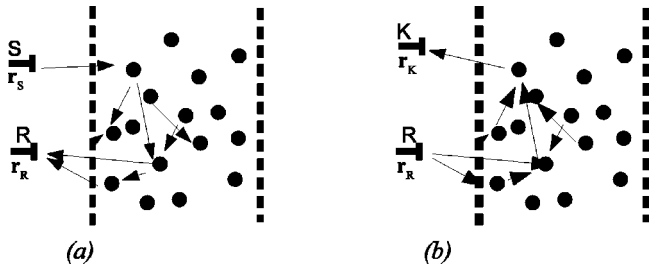

FIG. 14. The two steps of a one-channel TR experiment in a backscattering configuration through a multiple scattering medium. (a) Forward propagation step. (b) Backward propagation step.

$$\langle\Psi_{RT}(t)\rangle \underset{\Delta T\rightarrow 0}{=} \Delta T\xi_{t_0}(\mathbf{S},\mathbf{R},\mathbf{R},\mathbf{K},t). \quad (12)$$

The other interesting limit is when the time reversal window contains the whole recorded signal $\Psi(t)$, in which case

$$\langle\Psi_{RT}(t)\rangle \underset{\Delta T\rightarrow\infty}{=} \int \xi_\tau(\mathbf{S},\mathbf{R},\mathbf{R},\mathbf{K},t)d\tau. \quad (13)$$

So far the average TR field has been worked out. To this end, we have assumed that the first term of the right-hand side of Eq. (2) is negligible. If we do not neglect this term, the term $G_e(\mathbf{R}\rightarrow\mathbf{K};t)\otimes G_e(\mathbf{S}\rightarrow\mathbf{R};-t)\otimes f(-t)$ must be added to Eq. (5) as well as in the subsequent equations.

C. Variance of the TR

To determine the variance of the TR field, we have to average the squared time-reversed field. The coherent terms are neglected under the same conditions as those explained in the previous section. The complete derivation of the variance of the TR is described in [21]. However, due to the complexity of the complete expression, here it is only written in the limit of small TR windows:

$$\begin{aligned}\langle\Psi_{RT}(t)^2\rangle \underset{\Delta T\rightarrow 0}{=} \langle\Psi_{RT}(t)\rangle^2\\ + \Delta T\int \xi_{t_0}(\mathbf{S},\mathbf{R},\mathbf{S},\mathbf{R},\tau)\xi_{t_0+t}(\mathbf{K},\mathbf{R},\mathbf{K},\mathbf{R},\tau)d\tau\\ + \Delta T\int \xi_{t_0}(\mathbf{S},\mathbf{R},\mathbf{R},\mathbf{K},2t-\tau)\xi_{t_0}(\mathbf{S},\mathbf{R},\mathbf{R},\mathbf{K},\tau)d\tau. \quad (14)\end{aligned}$$

D. Approximation of the vertex

The vertex can be split into two distinct contributions [11]: the irreducible one (U) and the reducible one (R):

$$\begin{aligned}\langle\Theta(\mathbf{r}_1\rightarrow\mathbf{r}_2;t)\Theta(\mathbf{r}_{1'}\rightarrow\mathbf{r}_{2'};t)\rangle\\ = U(\mathbf{r}_1,\mathbf{r}_2,\mathbf{r}_{1'},\mathbf{r}_{2'};t) + R(\mathbf{r}_1,\mathbf{r}_2,\mathbf{r}_{1'},\mathbf{r}_{2'};t). \quad (15)\end{aligned}$$

The "Boltzmann approximation" consists in replacing (U) by the scattering by one scatterer (here noted S). This low-density approximation turns (R) into an incoherent multiple scattering series called "the ladder diagrams" which obey the

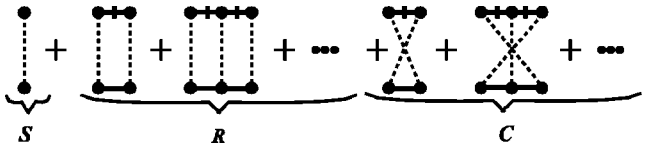

FIG. 15. Diagrammatic representation of the expansion of the vertex: (S) represents the single scattering contribution, (R) the "ladder diagrams," and (C) the most-crossed diagrams that restore reciprocity.

radiative transfer equation. (R) itself does not obey reciprocity. Therefore the Boltzmann approximation fails in describing any reciprocity-dependent effect, such as coherent backscattering. Beyond the Boltzmann approximation, reciprocity is restored by adding "most-crossed diagrams" (C), which are irreducible, to the diagrammatic expansion (see Fig. 15). It has been shown that the expressions of the ladder and most-crossed contributions are, respectively, $F_L(\mathbf{r}_1,\mathbf{r}_2;t)\delta(\mathbf{r}_1-\mathbf{r}_{1'})\delta(\mathbf{r}_2-\mathbf{r}_{2'})$ and $F_C(\mathbf{r}_1,\mathbf{r}_2;t)\delta(\mathbf{r}_1-\mathbf{r}_{2'})\delta(\mathbf{r}_2-\mathbf{r}_{1'})$ [10]. Obviously, due to the straightforward link between the vertex function and the ξ function [see Eq. (10)], the same decomposition occurs for ξ:

$$\begin{aligned}\xi_\tau(\mathbf{X}_1,\mathbf{X}_2,\mathbf{X}_3,\mathbf{X}_4,t) &= \xi_\tau^S(\mathbf{X}_1,\mathbf{X}_2,\mathbf{X}_3,\mathbf{X}_4,t)\\ &+ \xi_\tau^R(\mathbf{X}_1,\mathbf{X}_2,\mathbf{X}_3,\mathbf{X}_4,t)\\ &+ \xi_\tau^C(\mathbf{X}_1,\mathbf{X}_2,\mathbf{X}_3,\mathbf{X}_4,t).\end{aligned} \tag{16}$$

In the following, we shall neglect the single scattering contribution. The reciprocity symmetry means that all Green's functions are invariant upon permuting source and receiver positions: $G(\mathbf{r}_1\rightarrow\mathbf{r}_2;t)=G(\mathbf{r}_2\rightarrow\mathbf{r}_1;t)$. Consequently, in reciprocal media, a strong relation exists between the ladder and the most-crossed diagrams: $R(\mathbf{r}_1,\mathbf{r}_2,\mathbf{r}_{2'},\mathbf{r}_{1'};t)=C(\mathbf{r}_1,\mathbf{r}_2,\mathbf{r}_{1'},\mathbf{r}_{2'};t)$ or in other words $F_L(\mathbf{r}_1,\mathbf{r}_2;t)=F_C(\mathbf{r}_1,\mathbf{r}_2;t)=F(\mathbf{r}_1,\mathbf{r}_2;t)$. The same relation holds for ξ^C and ξ^R:

$$\xi_\tau^C(\mathbf{X}_1,\mathbf{X}_2,\mathbf{X}_3,\mathbf{X}_4,t)=\xi_\tau^R(\mathbf{X}_1,\mathbf{X}_2,\mathbf{X}_4,\mathbf{X}_3,t). \tag{17}$$

Using Eq. (10) gives

$$\begin{aligned}\xi_\tau^R(\mathbf{X}_1,\mathbf{X}_2,\mathbf{X}_3,\mathbf{X}_4,t) = \int & G_e(\mathbf{X}_1\rightarrow\mathbf{r}_1;-t)\otimes G_e(\mathbf{r}_2\rightarrow\mathbf{X}_2;-t)\\ &\otimes G_e(\mathbf{X}_3\rightarrow\mathbf{r}_1;t)\\ &\otimes G_e(\mathbf{r}_2\rightarrow\mathbf{X}_4;t)\\ &\otimes f(-t)F(\mathbf{r}_1,\mathbf{r}_2;\tau)d\mathbf{r}_1 d\mathbf{r}_2.\end{aligned} \tag{18}$$

Within the diffusion approximation, an analytical expression can be obtained for $F(\mathbf{r}_1,\mathbf{r}_2;t)$ [24]. The next two sections of the article will be devoted to elucidating the respective role of the reducible and the most-crossed components of the vertex function in TR focusing. First we will consider the transmission configuration and next the backscattering configuration which is more complicated.

IV. TRANSMISSION CONFIGURATION

A. Average TR field

In transmission, the points **S** and **R** are on opposite sides of the multiple scattering medium. The consequence is that $\xi_\tau^R(\mathbf{S},\mathbf{R},\mathbf{R},\mathbf{K},t)$ is null. Indeed, the effective Green's functions are appreciable only on a skin layer whose thickness is one or a few mean free paths. If $\mathbf{r}_1$ is in the skin layer at the sample input, then the effective Green function $G_e(\mathbf{S}\rightarrow\mathbf{r}_1;-t)$ is nonzero but in this case $G_e(\mathbf{R}\rightarrow\mathbf{r}_1;t)$ is negligible. Reciprocally, if $G_e(\mathbf{r}_2\rightarrow\mathbf{R};-t)$ is nonzero, $G_e(\mathbf{r}_2\rightarrow\mathbf{K};t)$ is zero. Therefore the average TR field [Eq. (11)] becomes

$$\langle\Psi_{RT}(t)\rangle=\int \xi_\tau^C(\mathbf{S},\mathbf{R},\mathbf{R},\mathbf{K};t)W\left(\frac{\tau-t_0}{\Delta T}\right)d\tau. \tag{19}$$

That is to say that in transmission TR focusing properties come only from the existence of the most-crossed diagrams. A visual interpretation of the effect of averaging over realizations on TR propagation is proposed in Fig. 16. The same kinds of conventions as used by Akkermans and Montambaux in Ref. [25] are adopted here. For clarity only propagation inside the multiple scattering medium is represented. An acoustic path starts from $\mathbf{r}_1$ and goes out at point $\mathbf{r}_2$. The wave is time reversed. The new path starts from $\mathbf{r}_3$ and exits at $\mathbf{r}_4$ with another phase. Time inversion is formally equivalent to replace the forward path by its conjugate (see Fig. 16). The average process cancels out most of these paths. The only remaining paths are those that propagate along the same trajectory during the forward and backward steps (i.e., $\mathbf{r}_1=\mathbf{r}_4$ and $\mathbf{r}_2=\mathbf{r}_3$; see Fig. 16). Moreover, the path and its conjugate have opposite propagation directions. It means that these paths will constructively interfere only if one of them can be replaced by its reciprocal. Thus the focusing only originates from the most-crossed diagrams that result from the reciprocity property. As the pairs of paths are linked by a convolution operator, they interfere constructively only at time $t=0$. Usually, in this kind of representation, a simple product operator replaces the convolution operator since one works in the frequency domain. Then constructive interferences occur at any time.

Therefore in transmission and on average, the TR focusing only succeeds thanks to reciprocity. In other words, only the most-crossed diagrams contribute to the average TR field. Usually the most-crossed diagrams are thought to be

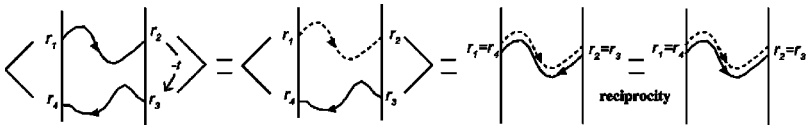

FIG. 16. Paths that contribute to the TR mean field in transmission configuration. Dotted line indicates the conjugated path.

significant only in backscattering; here we have shown that they play a fundamental role in transmission as well when a time reversal experiment is performed. Now let us consider the statistical fluctuations around the mean value.

B. Variance of the TR field

Using the reciprocity principle [Eq. (17)] and the observation that in transmission $\xi_\tau^R(\mathbf{S},\mathbf{R},\mathbf{R},\mathbf{K},t)$ vanishes, one infers that

$$\xi_\tau^C(\mathbf{S},\mathbf{R},\mathbf{K},\mathbf{R},t)=0. \tag{20}$$

Thus the second term of the variance in Eq. (14) only originates from the ladder contribution while the third term comes from the most-crossed diagrams. Again, a graphical interpretation is proposed in Fig. 17 In the symbolic equation represented in Fig. 17, there are now four paths in each term: two correspond (solid line) to the forth and back propagation in the TR process and the other two symbolize the conjugate paths required to compute the square of the TR field. The three terms of the figure correspond to the three terms on the right-hand side of Eq. (14). The first one denotes the square of the average value of the TR field. The second one corresponds to the contribution of the forward path (from $\mathbf{r}_1$ to $\mathbf{r}_2$) with its conjugate together with the backward (from $\mathbf{r}_3$ to $\mathbf{r}_4$) path and its conjugate. The propagation directions of paths in each pair are the same. This means that the second contribution does not involve reciprocity of the medium. These two paths are linked together by a simple product operator and is therefore a background contribution that slowly changes with time. The third term due to reciprocity only appears at the focusing ($t\approx 0$ and around $\mathbf{K}=\mathbf{S}$).

V. BACKSCATTERING CONFIGURATION

In the backscattering configuration, $\xi_\tau^R(\mathbf{S},\mathbf{R},\mathbf{R},\mathbf{K},t)$ can be nonzero when **S** and **K** are both close to **R**. In order to illustrate the theoretical results obtained in the backscattering configuration and to compare them later to experiment, we will consider an explicit solution for the ξ function. In the general case, the computation of ξ is very complex. However, it can be greatly simplified if we assume that all active elements (**S**, **R**, and **K**) are in the far field zone of the multiple scattering medium and that the initial pulse $f(t)$ has a bandwidth much smaller than its central frequency. Under these conditions, ξ is written as

$$\xi_\tau(\mathbf{X}_1,\mathbf{X}_2,\mathbf{X}_3,\mathbf{X}_4;t)=[\tilde{F}'(\mathbf{X}_4-\mathbf{X}_1,\mathbf{X}_3-\mathbf{X}_2;\tau)+\tilde{F}'(\mathbf{X}_3-\mathbf{X}_1,\mathbf{X}_4-\mathbf{X}_2;\tau)]f(-t), \tag{21}$$

where $\tilde{F}'$ is the 2D-spatial Fourier transform of F' which is a function directly linked to F (see Ref. [21] for more details) introduced in Eq. (18) as a solution of the diffusion equation with boundary conditions and calculated recently [26]. The computation is quite long and complex and is out of the scope of this article. We have applied these results using parameters that correspond to our experimental ultrasonic experiment performed in a water tank. The central frequency of the initial pulse is 3.5 MHz, the sound speed in the homogeneous medium is $c=1.5$ mm/μs, and the thickness of the multiple scattering medium is 35 mm. The diffusion coefficient is $D=3.2$ mm^2/μs, the elastic mean free path is $\ell=4$ mm, and the transport mean free path is $\ell^*=4.8$ mm [16].

A. Average TR field

From Eqs. (11) and (16) the average time-reversed field involves now both the ladder and the most-crossed diagram contributions. They are represented in terms of paths in Fig. 18. The contribution I due to crossed diagrams corresponds to the one previously considered in transmission. However when the four points $\mathbf{r}_i$ are at the same location, the second contribution (II) adds up to the previous one. It describes constructive interferences between a path and its conjugate that follows the same sequence of scattering events in the same order. As the direction of propagation is the same along both paths, this contribution would survive even if reciprocity was broken. Both contributions show up only around time $t=0$. The spatial focusing including these two terms is plotted in Fig. 19. The ladder diagrams (contribution II in Fig. 18) only contribute when **S**, **R**, and **K** are sufficiently close to each other. The reciprocity principle links each ladder diagram to a crossed one. Therefore the amplitude of the TR peak is twice higher when the TR channel and the source coincide (see Fig. 20). This behavior is very similar to the coherent backscattering effect. More details are given in Sec. VIII. A surprising conclusion can be already drawn: when reciprocity is broken—for instance, by a strong flow—TR focusing still works as long as the initial source and the TR channel are at the same position. This is contrary to the intuitive idea that time reversal focusing requires at least reciprocity of the medium. These theoretical results are in good agreement with the experimental ones (Figs. 7 and 8).

B. Variance of the TR field

The expression of the variance of Ψ_{RT} is quite complex. Indeed, the variance is composed of not fewer than eight terms. Nevertheless, in the far field limit and for short TR

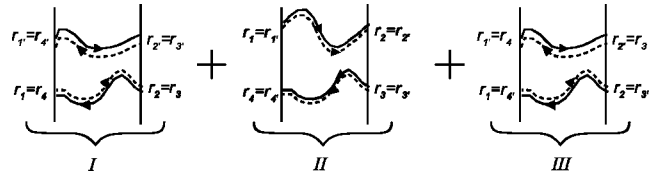

FIG. 17. Paths that contribute to the average squared TR field.

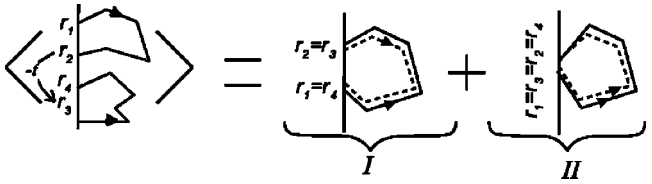

FIG. 18. Paths contributing to the average TR field in backscattering.

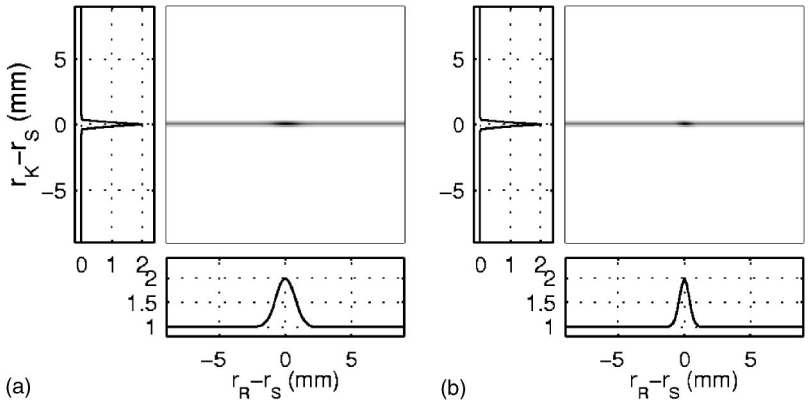

FIG. 19. Numerical computation of the spatial dependence of the average TR wave field at time $t=0$ versus the distance between the source and the measurement points (vertical scale) and the distance between TR channel and the initial source (horizontal scale). The representations are in linear gray scale. The vertical curve is the plot of the field for $\mathbf{R}=\mathbf{S}$ and the horizontal one for $\mathbf{K}=\mathbf{S}$. (a) and (b) correspond to TR focusing for time reversal windows, respectively, centered at 15 and 55 μs.

windows, its expression is greatly simplified [Eqs. (14) and (21)]:

$$\langle \Psi_{RT}(t)^2\rangle - \langle \Psi_{RT}(t)\rangle^2 \underset{\Delta T\to 0}{=} [\tilde{F}'(0,0;t_0)+\tilde{F}'(\mathbf{R}-\mathbf{S},\mathbf{R}-\mathbf{S};t_0)] \times [\tilde{F}'(0,0;t_0+t)+\tilde{F}'(\mathbf{R}-\mathbf{K},\mathbf{R}-\mathbf{K};t_0+t)]\Delta T\int f(\tau)^2 d\tau + [\tilde{F}'(\mathbf{K}-\mathbf{S},0;t_0)+\tilde{F}'(\mathbf{R}-\mathbf{S},\mathbf{K}-\mathbf{R};t_0)]^2\Delta T[f(-t)\otimes f(-t)](2t). \quad (22)$$

The variance reduces to the sum of two terms. The first one represents a slowly varying contribution. If the source and the TR channel positions are identical ($\mathbf{R}=\mathbf{S}$), this term is twice higher than if they would have been far away from each other. The same conclusion applies when the TR channel and the recording point are identical ($\mathbf{R}=\mathbf{K}$). Thus when all three points coincide, we expect the variance to be enhanced by a factor of 4.

The second term oscillates twice faster than the central frequency of the initial pulse. This term is significant only at the focus location ($\mathbf{S}$) and at the focus time ($t=0$). Moreover, when the three points are all at the same location, this term is also enhanced by a factor of 4. Altogether the variance can be enhanced by a factor of up to 8. Figure 21 shows the spatial dependence of the variance at three different times for which the oscillating term is, respectively, minimum, zero, and maximum. These plots are fully comparable to the experimental ones (see Figs. 11 and 12).

In conclusion, we have found three contributions to the variance of the TR field at backscattering. The first one is a spatially uniform background due to the ladder diagrams. In addition to this the most-crossed diagrams are responsible for a "diagonal enhancement" ($\mathbf{R}=\mathbf{K}$) and a "vertical enhancement" ($\mathbf{R}=\mathbf{S}$) (see Fig. 21). Now we have complete expressions and diagrammatic interpretations for the mean value and the variance of the TR field in transmission as well as in backscattering. In the next two sections, we apply these results to demonstrate "hyperfocusing" and "self-averaging" within the framework of the self-consistent diagrammatic approach. Finally we establish the link between TR focusing and CBS.

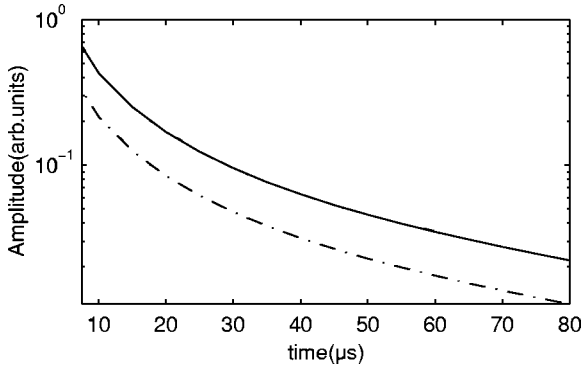

FIG. 20. Evolutions of the average time-reversed peak amplitude recorded at the source ($\mathbf{K}=\mathbf{S}$) with respect to the center of the TR window (time t_0). Solid line: TR channel is at the same position as the source ($\mathbf{S}=\mathbf{R}=\mathbf{K}$). Dashed line: $\mathbf{S}$ and $\mathbf{R}$ are far away from each other.

VI. HYPERFOCUSING

One of the most striking effects in one-channel TR inside scattering or reverberant media is the hyperfocusing effect [2,4,6,27,28]. Resolutions of about one wavelength have been experimentally observed. In transmission, we can interpret this effect using Eqs. (17)–(19). Indeed the average TR field can be seen as a converging field emerging from an aperture function given by $O(\mathbf{r}_1)=\int\{\int F(\mathbf{r}_1,\mathbf{r}_2;\tau) \times W[(\tau-t_0)/\Delta T]d\tau\}G_e(\mathbf{R}\to\mathbf{r}_2;t)\otimes G_e(\mathbf{r}_2\to\mathbf{R};-t)\otimes f(-t) \times d\mathbf{r}_2$ where $\mathbf{r}_1$ is the coordinate on the virtual lens. The maximum width of $O(\mathbf{r}_1)$ is the transverse dimension of the sample. For an infinite slab, half-wavelength resolution is achieved with only a single-channel TR. From a practical

point of view, if the source is not really point like, its angular spectrum sets the lower limit for the spatial resolution. In backscattering, the same formalism can be applied.

VII. SELF-AVERAGING PROPERTY OF TR

The time-reversed signal at the focusing point ($\mathbf{S}$) consists of a short pulse surrounded by sidelobes that fluctuate from one realization of disorder to the other. We define the signal-to-noise ratio (SNR) at the focusing location ($\mathbf{K}=\mathbf{S}$) as the intensity of the peak (at $t=0$) divided by the variance next to the peak. In other words, $\mathrm{SNR}=\langle\Psi_{RT}(0)\rangle^2/\langle\Psi_{RT}(t)^2\rangle$. Giving a general expression of the SNR is quite complex. However, if the initial excitation function $f(t)$ is narrow band and frequency-dependent dissipation is negligible, then $G_e(\mathbf{S}\rightarrow\mathbf{r}_1;-t)\otimes G_e(\mathbf{r}_1\rightarrow\mathbf{S};t)$ behaves as a Dirac $\delta(t)$. In that case the SNR becomes for short and long time-reversal windows, respectively,

$$\mathrm{SNR}\underset{\Delta T\rightarrow 0}{=}\frac{\Delta T f^2(0)}{\int f^2(t)dt} \tag{23}$$

and

$$\mathrm{SNR}\underset{\Delta T\rightarrow\infty}{=}\frac{f^2(0)}{\int f^2(t)dt}\frac{\left[\int F(\mathbf{r}_1,\mathbf{r}_2,\tau)d\mathbf{r}_1d\mathbf{r}_2d\tau\right]^2}{\int F(\mathbf{r}_1,\mathbf{r}_2,\tau)^2d\tau d\mathbf{r}_1d\mathbf{r}_2}. \tag{24}$$

Equation (23) is equal to the ratio between the duration of the time reversal window and the one of the initial pulse $f(t)$. As for Eq. (24), it represents the ratio of the time spreading of the initial pulse due to diffusion and the pulse duration. Hence for small TR windows the SNR ratio increases linearly with respect to the TR window length and reaches a plateau for large TR windows. This result, established here within multiple scattering theory, has been also found from phenomenological assumptions in several previous papers (e.g., [3]). Expressions (23) and (24) also show that the SNR increases as the pulse length decreases—i.e., when the bandwidth is enlarged. Broadband time reversal focusing in a complex medium tends to be a self-averaging process: the TR field obtained on one realization of disorder is a good estimator of its average field, provided that frequency-dependent dissipation is neglected. An experimental illustration has been provided in Sec. II (Figs. 3 and 4).

VIII. TIME REVERSAL AT BACKSCATTERING vs CBS

To record the CBS in an acoustic experiment [20,26], a source located at $\mathbf{S}$ sends out a short pulse into a multiple scattering medium. The average reflected intensity is recorded at time t_0 for each point $\mathbf{R}$:

$$I=\langle G(\mathbf{S}\rightarrow\mathbf{R};t_0)^2\rangle\approx\xi_{t_0}(\mathbf{S},\mathbf{R},\mathbf{S},\mathbf{R},t=0). \tag{25}$$

This expression defines the spatial distribution of the backscattered intensity at a given time. Interestingly, the average TR field for $\mathbf{S}=\mathbf{K}$ and at $t=0$ reads

$$\langle\Psi_{RT}(t)\rangle=\Delta T\xi_{t_0}(\mathbf{S},\mathbf{R},\mathbf{R},\mathbf{S},t=0). \tag{26}$$

The expression of the average TR field is very close to the expression of the average backscattered intensity [Eq. (25)]. Yet the exact equality is obtained only if the third and fourth entries are permuted. The physical signification of this permutation is fundamental. It implies that from TR to CBS, the roles of the ladder and most-crossed diagrams are exchanged: in the CBS, the "background" and "enhancement" intensities are, respectively, due to the ladder and the most-crossed diagrams, while in the average TR field, the background originates from the most-crossed diagrams and the enhancement from the ladders.

This property appears more explicitly in the diagrammatic representations of the average intensity on the one hand and the average TR field amplitude on the other hand (Fig. 22). Let us recall the conventions of diagrammatic representations. First, the sources are on the left part of the diagrams while the receivers are on the right part. Roughly, a dot can be interpreted as a scattering point and two dots linked by a dashed line represent the same scatterer. A thick segment between two dots or between a dot and one of the four outer positions symbolizes the effective Green's function; it is barred to indicate complex conjugation. The four outer positions are classified in two pairs: two positions form a pair if they are linked to the same scatterer by two Green's functions, one of them being conjugated. A rule exists to deter-

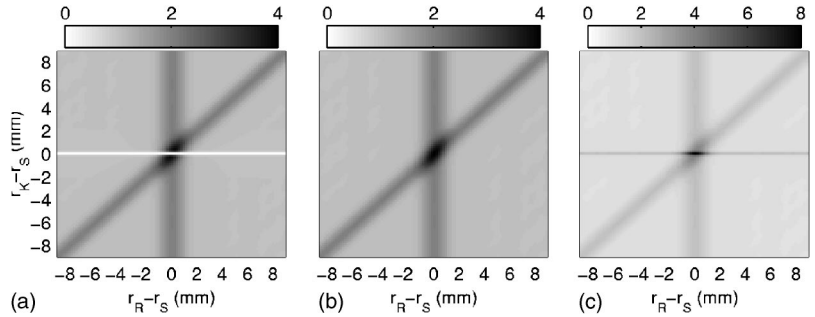

FIG. 21. Three grey level representations of the variance. The vertical scale is the distance between the observer $\mathbf{K}$ and the source $\mathbf{S}$. The horizontal scale is the distance between the TR channel $\mathbf{R}$ and the initial source $\mathbf{S}$. The time reversal window is centered at $t_0=15$ μs. (a), (b), and (c) represent the variance at three different times for which the oscillating term is, respectively, minimum, zero, and maximum.

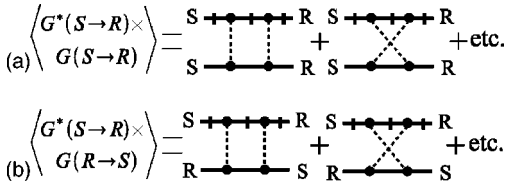

FIG. 22. Diagrammatic representation of the intensity (a) and the time reversal amplitude at the focal spot (b). On the left part of the diagrams are represented the position of the two sources: twice **S** in (a), **S** and **R** in (b). On the right part of the diagrams are represented the positions of the two receivers: twice **R** in (a), **R** and **S** in (b). Only second-order diagrams are drawn here. The left diagrams correspond to the ladder contribution and the right ones to the most-crossed contribution.

mine whether a diagram is significant or not. A diagram will be significant only if the two positions of each pair are sufficiently close and the contribution will reach its maximum when the two positions are identical. Hence, in the case of the intensity [Fig. 22(a)], the well-known result is retrieved: the ladders contribute whatever the distance between **R** and **S** whereas the most-crossed diagrams are only significant when $\mathbf{R}\approx\mathbf{S}$. In the case of TR, the role of diagrams are now exchanged [Fig. 22(b)]: the crossed ones always contribute to the focusing amplitude whatever the distance between **R** and **S**. As to the ladders, they only arise when $\mathbf{R}\approx\mathbf{S}$.

A direct consequence is that in a nonreciprocal medium the "enhancement" of the TR average field would remain, whereas the background would vanish. On the contrary, the enhancement of the backscattered intensity (i.e., CBS) would disappear, whereas the background would remain.

IX. CONCLUSIONS

One-channel time reversal experiments have been reexamined within the framework of the multiple scattering theory. On the one hand, previously established results such as hyperfocusing and self-averaging have been rigorously demonstrated within this theoretical framework. On the other hand, the link between one-channel TR and CBS has been established. Especially, we have shown that when the initial source and the time reversal point coincide, the time-reversed amplitude is twice as large. Surprisingly, this enhancement is due to the ladder diagrams and not to the most-crossed ones, contrary to CBS. These theoretical predictions have been confirmed by experimental results which have been obtained with ultrasonic waves propagating through a random 2D collection of parallel steel rods. The generalization to multiple-channel TR and to random media subject to long-range correlations will be the object of further studies.

ACKNOWLEDGMENTS

The authors wish to acknowledge David Lacoste for fruitful discussions as well as the GDR IMCODE of CNRS for its financial support.

[1] A. Derode, P. Roux, and M. Fink, Phys. Rev. Lett. **75**, 4206 (1995).
[2] D.R. Dowling and D.R. Jackson, J. Acoust. Soc. Am. **91**, 3257 (1992).
[3] A. Derode, A. Tourin, and M. Fink, J. Appl. Phys. **85**, 6343 (1999).
[4] A. Derode, A. Tourin, and M. Fink, J. Acoust. Soc. Am. **107**, 2987 (2000).
[5] A. Derode, A. Tourin, and M. Fink, Phys. Rev. E **64**, 036606 (2001).
[6] Peter Blomgren and George Papanicolaou, J. Acoust. Soc. Am. **111**, 230 (2001).
[7] F.D. Tappert, in *Workshop on Wave Propagation and Underwater Acoustics*, edited by Joseph B. Keller and John S. Papadakis, *Lecture Notes in Physics*, Vol. 70 (Springer, New York, 1977), p. 224.
[8] G. Maret and P.E. Wolf, Z. Phys. B: Condens. Matter **65**, 409 (1987).
[9] D.J. Pine, D.A. Weitz, P.M. Chaikin, and E. Herbolzheimer, Phys. Rev. Lett. **60**, 1134 (1988).
[10] D.S. Wiersma, P. Bartolini, A. Lagendijk, and R. Righini, Nature (London) **390**, 671 (1997).
[11] B.A. van Tiggelen, in *Diffuse Waves in Complex Media*, edited by Jean-Pierre Fouque, Vol. 531 of *NATO Advanced Study Institute, Series C: Mathematical and Physical Sciences* (Kluwer Academic, Dordrecht, 1999), pp. 1–60.
[12] R. Berkovits and S. Feng, Phys. Rep. **238**, 135 (1994).
[13] B.A. van Tiggelen, Phys. Rev. Lett. **91**, 243904 (2003).
[14] Meint P. Van Albada and Ad Lagendijk, Phys. Rev. Lett. **55**, 2692 (1985).
[15] Pierre-Etienne Wolf and Georg Maret, Phys. Rev. Lett. **55**, 2696 (1985).
[16] A. Tourin, A. Derode, A. Peyre, and M. Fink, J. Acoust. Soc. Am. **108**, 503 (2000).
[17] K.M. Watson, J. Math. Phys. **10**, 688 (1967).
[18] D.A. de Wolf, IEEE Trans. Antennas Propag. **AP-19**, 254 (1971).
[19] Yu.N. Barabanenkov, Izv. Vyssh. Uchebn. Zaved., Radiofiz. **16**, 88 (1973).
[20] A. Tourin, P. Roux, A. Derode, B.A. van Tiggelen, and M. Fink, Phys. Rev. Lett. **79**, 3637 (1997).
[21] See EPAPS Document No. E-PLEEE8-70-087407 for materials supplemental to this paper illustrating the relation between time reversal focusing and coherent backscattering in multiple scattering media: a diagrammatic approach. A short introduction of the Green's functions formalism inside a multiple scattering medium is proposed, the complete mathematical derivation of the variance of the time-reversed field is presented. Finally details about the far field approximation are provided. A direct link to this document may be found in the online article's HTML reference section. The document may also be reached via the EPAPS homepage (http://www.aip.org/pubservs/epaps.html) or from ftp.aip.org in the directory /epaps/. See the EPAPS homepage for more information.

[22] Ping Sheng, *Introduction to Wave Scattering, Localization, and Mesoscopic Phenomena* (Academic, San Diego, 1995).
[23] P.C. Waterman and R. Truell, J. Math. Phys. **2**, 512 (1961).
[24] Martin B. van der Mark, Meint P. van Albada, and Ad Lagendijk, Phys. Rev. B **37**, 3575 (1988).
[25] E. Akkermans and G. Montambaux, in *Wave Scattering in Complex Media: From Theory to Application*, edited by B. van Tiggelen and Sergey Skipetrov, Vol. 107 of *NATO Advanced Study Institute, Series II: Mathematics, Physics and Chemistry* (Kluwer Academic, Dordrecht, 2003), pp. 101–123.
[26] Arnaud Tourin, Ph.D. thesis, Université Denis Diderot, 1999.
[27] C. Draeger and M. Fink, Phys. Rev. Lett. **79**, 407 (1997).
[28] A. Tourin, A. Derode, and M. Fink, Europhys. Lett. **47**, 175 (1999).